Journal of Thermal Science Vol.33, No.3 (2024) 1148−1160

https://doi.org/10.1007/s11630-024-1912-5 **Article ID: 1003-2169(2024)03-1148-13**

Heat Transfer Characteristics of a Microchannel Heat Sink with Highly-Dense Micro-Jet Arrays

ZHANG Yu[1], CHEN Xiaoyan[2], MIAO Lin[2], CHEN Liang[1*], HOU Yu[1]

1. State Key Laboratory of Multiphase Flow in Power Engineering, Xi'an Jiaotong University, Xi'an 710049, China
2. Beijing Aerospace Technology Institute, Beijing 100083, China

Abstract: This paper proposed a new structure of highly-dense micro-jet arrays for hybrid jet-impingement/microchannel heat sinks (~120 jet per cm^2 with jet width of 0.35 mm). Parametric study is performed to investigate the influence of structure and flow parameters on the convective heat transfer of water jet cooling in confined space. The simulation results show that the optimal jet width, jet spacing and impingement distance are around 0.2 mm, 0.2 mm and 0.3 mm, respectively, which can achieve a low thermal resistance as well as a relatively low pressure drop. The analysis of the heat transfer pathways shows that the micro-fin jet structures can extend the impinging heat transfer area and conduct a considerable proportion of heat, which can reach up to 38.9% with the Reynolds number ranging from 797.1 to 5602.2. The heat transfer characteristics in the heat sink will shift from impingement dominated heat transfer to the channel-convection dominated heat transfer as the jet impingement distance increases. A correlation is proposed to predict the average Nusselt number on the stagnation area for the heat sink with different structure parameters, and the deviations of predictions from the numerical results are less than 10%.

Keywords: hybrid heat sink; impingement; microchannel; thermal management; high heat flux

1. Introduction

With the downscaling of electronic components, the increase of power density leads to problems such as high heat flux heat dissipation and local hot spots, which pose a severe challenge to efficient thermal management technology [1]. Microchannel and micro-jet are two powerful methods to cool the hot surface of high-power electronic equipment. As early as 1981, Tuckerman and Pease proposed a structure of a parallel flow microchannel heat sink to dissipate 790 W/cm^2 heat flux through single-phase water, but it brought a high pressure drop of 214 kPa [2]. Many works have been performed to optimize the microchannel heat sink structure including inlet shapes [3–5], wall roughness [6], micro-structures of the heating surface [7–12] and channel arrangement [13–16]. Although it is capable of dissipating high heat flux while maintaining the single-phase state of the working fluid, the large pressure drop and temperature gradient on the cooling surface cannot be ignored. For micro-jet cooling, the fluid flows through jets and radially impinges to the impacted surface to cool the hot surface [17]. The jet-impingement method has a better cooling performance around the impact region (stagnation region) [18] where the high convective heat transfer rate occurs, but it drops rapidly away from the

Received: May 08, 2023
AE: FAN Liwu
Corresponding author: CHEN Liang E-mail: liangchen@xjtu.edu.cn

Nomenclature

c_p	specific heat capacity of fluid/J·(kg·K)$^{-1}$	q''	heat flux on the heating surface/ MW·m^{-2}
D_{imp}	impingement distance/mm	Re	jet inlet Reynolds number
D_p	plate thickness/mm	T_{in}	inlet temperature/K
k_f, k_s	the thermal conductivity of fluid and solid/W·(m·K)$^{-1}$	$T_{max/min/ave}$	maximum/minimum/average heating surface temperature/K
L_{hpt}	distance of the jet impact surface to the heating surface/mm	T_{out}	average temperature of the outlet/K
L_{jet}	jet inlet length/mm	$\vec{U}$	flow velocity/m·s^{-1}
m_{in}	total inlet flow rate/L·min^{-1}	W_{jet}	jet width/mm
Nu_0	Nusselt number of the stagnation area	W_{js}	jet spacing/mm
P_{in}	inlet pressure/Pa	W_s	sum of jet width and jet spacing/mm
ΔP_{max}	maximum pressure drop from inle to outlet/Pa	θ_{tr}	thermal resistance/K·m^2·MW^{-1}
Pr	Prandtl number	μ	viscosity/Pa·s
Q_{pp}	pumping power/W	ρ	fluid density/kg·m^{-3}

stagnation point, which leads to non-uniform distribution of surface temperature.

In the single-phase heat transfer regime, for both the microchannel and jet-impingement heat sink, the mass flux has to be increased in order to achieve a higher heat flux and temperature homogeneity, which lead to a large pressure drop and pump power. Therefore, various hybrid heat sinks have been proposed which combines the jet-impingement and microchannel structures [19–21]. Cui [22] proposed two submerged jet impingement microchannel heat sinks with straight ribs (SJIMHS) and oblique ribs (OJIMHS). And the results show that OJIMHS achieves better heat transfer performance. When the flow rate is 0.5 L/min and the heat flux is 100 W/cm², the average temperature of the heat transfer surface is lower than 60°C and the averaged heat transfer coefficient is 2.8 W/(cm^2·K) of OJIMHS under the inlet fluid temperature of 283 K and flow rate of 2.5 L/min in the experiment. In order to show the better heat dissipation ability of hybrid heat sink, the heat transfer performance of hybrid jet/impingement microchannel heat sink was compared with that of traditional microchannel in many works. Jang et al. [23] made an experimental comparison between a traditional parallel flow microchannel heat sink with a hybrid heat sink of both microchannel and jet-impingement structure. It was found that the thermal resistance was 152.5 K·m^2/MW with a pump power of 0.072 W, while it was 296.25 K·m^2/MW for the parallel flow heat sink. The cooling performance of microchannel heat sink under the action of impact flow was about 48.5% higher than that of parallel flow heat sink. Lelea et al. [24] proposed numerical comparison method to study the performance of tangential jet-impingement microchannel heat sinks and the conventional heat sinks. The results show that adding jet parts can achieve a lower average temperature and better temperature distribution. Loganathan et al. [25] showed that combining microchannel with jet-impingement is one of the most effective methods to optimize the efficiency of microchannel heat sink. The influence of the size and inclination of the secondary inlet on the performance of the microchannel heat sink was numerically studied. The results show that the lower wall temperature and better insulation effect can be achieved by adding the jet parts.

Compared with the conventional micro-channel or micro-jet heat sinks, two strategies combined together can achieve better cooling performance, but the temperature homogeneity is still not desirable due to the sparse distribution of jets. The key to improve the cooling ability is to reduce the size of jet and increase the jet density. In our work, a hybrid heat sink structure of highly-dense micro-jet array and microchannels is proposed, and the heat sink cooling ability is numerically investigated. Due to the highly-dense micro-jet array (~120 jet per cm^2) and the separate design of inflow and outflow passages, the hybrid structure can achieve a thermal resistance of 5.94 m^2·K/MW while maintaining a good heating surface temperature distribution when dissipating high heat flux up to 1.5 MW/m^2 with the inlet flow rate 3 L/min.

2. Numerical Methods

2.1 Geometric model

The proposed heat sink is composed of a series of copper plates welded together with one whole inlet and outlet. As shown in Fig. 1, the inflow plate and outlet guide plate are used for flow distribution as the coolant

flows in and out, respectively. The division plate is used to direct the coolant into the microchannel heat exchanger plate. One group of stacked plates composes of six copper plates (1, 2, 3, 4, 2, 1) and series of single-group stacked plates are welded together as a whole heat sink. For simulation, only one group of stacked plates is chosen.

Ignoring the diversion structure, only the heat transfer part of the jet/impingement microchannel heat sink is simulated (shown in Fig. 2(a) dotted lines). Owing to the symmetry of the structure, an entire inlet passage and two halves of the wall on both sides are selected in one simulation unit (denoted as dotted lines in Fig. 2(b)). Because this unit in Fig. 2(c) is symmetrical with respective to the middle plane and half of the outlet is chosen (denoted as dotted lines in Fig. 2(c)), it can be further simplified and one half (Fig. 2(d)) is selected as the simulation domain. Water is used as the working fluid to dissipate high heat flux.

2.2 Governing equations and solution procedure

In the present study, a steady-state and single-phase flow is assumed. The cooling medium is water with an inlet temperature of 300 K. The continuous, momentum and energy conservation equations of the fluid domain are as follows.

$$\nabla\cdot\vec{U}=0 \tag{1}$$

$$\left(\vec{U}\cdot\nabla\right)\rho\vec{U}=-\nabla P+\mu\nabla^2\vec{U} \tag{2}$$

$$\rho c_p\left(\vec{U}\cdot\nabla T\right)=k_{\mathrm{f}}\nabla^2T \tag{3}$$

Energy equation of the solid substrate and micro-fins:

$$k_{\mathrm{s}}\nabla^2T=0 \tag{4}$$

where $\vec{U}$ is the fluid flow velocity, m/s; ρ is the fluid density, kg/m^3; P is the pressure, Pa; μ is the viscosity, Pa·s; c_p is the specific heat capacity of fluid, J/(kg·K); k_{f} and k_{s} are the thermal conductivity of fluid and solid, respectively, W/(m·K). The material of solid part is

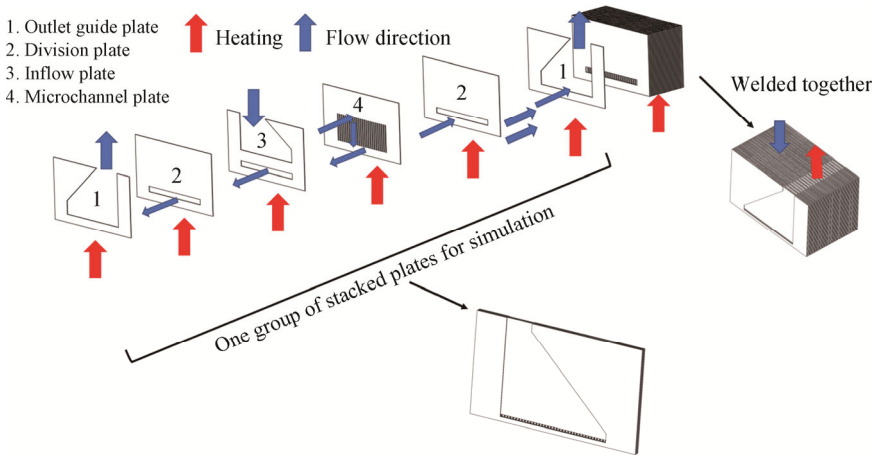

Fig. 1 Components of jet impingement microchannel

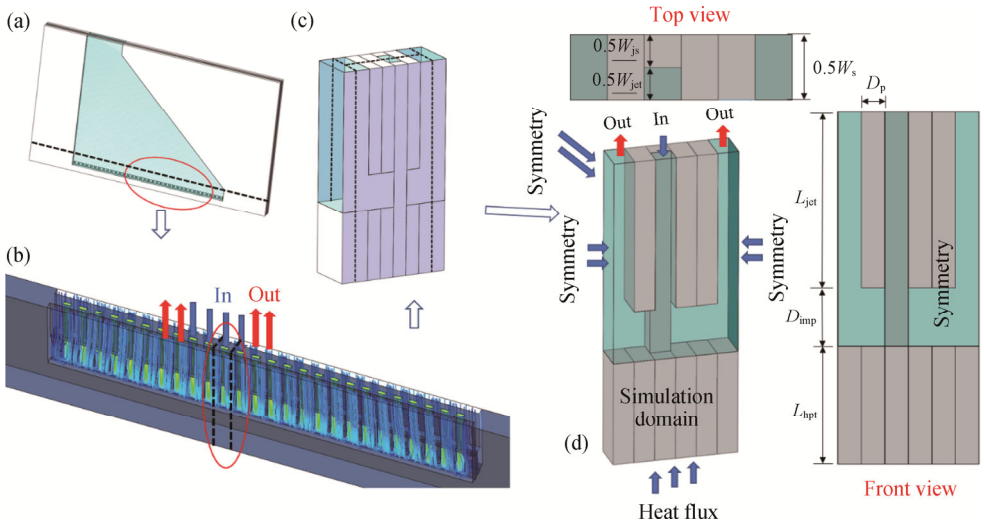

Fig. 2 Selecting the appropriate geometric model for modeling

oxygen free copper with constant physical properties and piecewise linear fittings are used for the fluid properties.

The thermal resistance and the convective heat transfer coefficient of the jet-impingement microchannel heat sink are used to detect the flow and heat transfer performance. The thermal resistance is determined by the followed equation:

$$\theta_{tr} = \frac{T_{ave} - T_{in}}{q''} \tag{5}$$

where, θ_{tr} is thermal resistance, K·m^2/MW; T_{ave} is the average temperature of the heating surface, K; T_{in} is the inlet fluid temperature, K; q'' is the heat flux on the heating surface, MW/m^2.

The convective heat transfer coefficient of the jet-impingement microchannel heat sink along the center line through the impinged area is determined by the followed equation:

$$h_{cov} = \frac{q''}{T_{imp} - T_{in}} \tag{6}$$

where, T_{imp} is the temperature of the centre line through the impinged area, K; T_{in} is the inlet fluid temperature, K; q'' is the heat flux on the heating surface, MW/m^2.

The Nusselt number Nu of the stagnation area and the pumping power Q_{pp} of the heat sink are formed by the following equations to evaluate the thermal performance of the jet impingement microchannel heat sink:

$$Nu = \frac{h_{cov} \cdot L}{k_f} \tag{7}$$

$$Q_{pp} = \Delta P_{max} \cdot m_{in} \tag{8}$$

where, L is the characteristic length of the heat sink inlet; ΔP_{max} is the maximum pressure drop between the inlet and outlet and m_{in} is the inlet flow rate of the heat sink.

The total inlet flow rate of the designed heat sink (six main copper plates) is 1 L/min with the temperature of 300 K. As shown in Fig. 2(d), the wall boundary on the top of the structure domain is adiabatic; the coupled boundary conditions are applied at walls in contact with the fluid domain; gauge pressure outlet condition is used for the microchannel outlet and heating surface heat flux is 1.5 MW/m^2. Symmetrical boundary consitions are applied for the other fluid and solid boundaries. In the baseline simulation, the following structure parameters are used, W_{jet}=W_{js}=0.35 mm, W_s=0.7 mm, T_p=0.2 mm, L_{jet}=1.5 mm, D_{imp}=0.5 mm, L_{hpt}=1.0 mm. We use "W_{jet}×L_{jet}-D_{imp}-L_{hpt}" as the naming rule of different structures. For example, the baseline structure is named as "0.35×1.5-0.5-1.0".

2.3 Grid independence test

Simulations are implemented in ANSYS FLUENT 17.0, and the standard k-ω turbulence model is employed. The pressure-velocity coupling is solved with the SIMPLE scheme, and the Green-Gauss Node Based scheme is used for gradient evaluation. The momentum equations, turbulence equations and energy equations are discretized by using second order upwind scheme. Structured grids are used for the simulation domain, and the near wall meshes are refined as shown in Fig. 3. There are two grid independence tests in this study including numerical simulation of our work and the experimental vertification. The mesh dependence is examined with both four grid systems shown in Table 1(a) and (b) from the number of 238 180 to 1 500 965 and from 137 123 to 1 152 480, respectively. The relative variations of average heating surface temperature are calculated under 1.5 MW/m^2 heat flux density with inlet flow rate 0.014 L/min and the working condition in Fig. 4 (the model validation). $\left|X^j - X^{j+1}\right| / X^j \le 5\times10^{-5}$ is selected as the criterion for grid independence

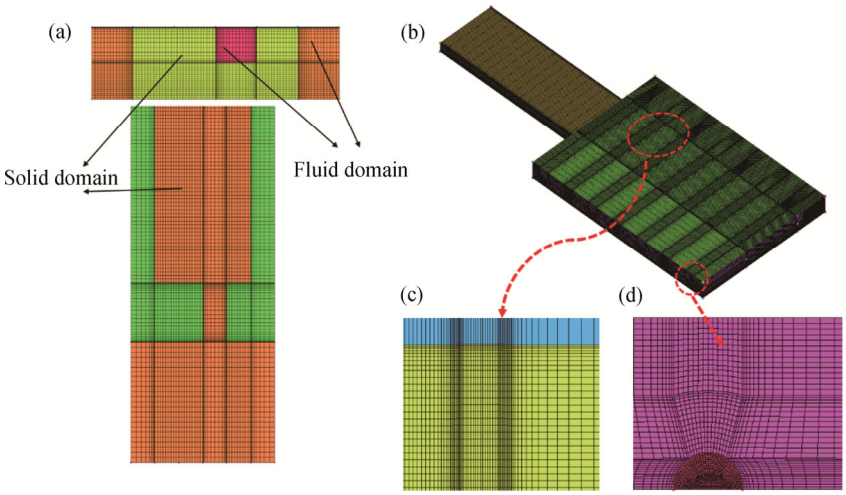

Fig. 3 Grid generations of the simulation domain of (a) our work and (b, c and d) experimental vertification

verification. According to results shown in Table 1(a) and (b), Mesh 3 of 928 500 cells and Mesh 7 of 613 409 are employed in the following calculations.

Table 1 Grid independence verification

Case	Number of cells	T_{ave}/K	$\left\|T_{ave}^{j} - T_{ave}^{j+1}\right\| / T_{ave}^{j}$
(a) Results of grid independence test of our study			
Mesh 1	238 180	371.8737	
Mesh 2	520 935	371.7016	4.63×10^{-4}
Mesh 3	928 500	371.6737	7.51×10^{-5}
Mesh 4	1 500 965	371.6700	9.96×10^{-6}
(b) Results of grid independence verification of experimental validation			
Mesh 5	137 123	348.6545	
Mesh 6	351 832	345.6702	8.6×10^{-3}
Mesh 7	613 409	345.1884	1.45×10^{-3}
Mesh 8	1 152 480	345.1698	5.4×10^{-5}

2.4 Model validation

Jet flow in microchannels is always complicated and highly turbulent. In our study, the inlet jet Reynoldes number Re_{jet} is about 1601. According to Revill [26], Re_{jet}=1601 is fully turbulent and the laminar flow model is not applicable here. The experimental data in Myung Ki Sung and Issam Mudawar [19, 27] are chosen to validate the simulations using standard k-ω turbulence model as shown in Fig. 4. They proposed a hybrid cooling scheme that combines the cooling benefits of micro-channel flow and micro-circular-jet-impingement. With this hybrid cooling scheme, the coolant is introduced gradually as a series of jets into each micro-channel of a micro-channel heat sink, and is expelled symmetrically through both ends of the micro-channel. Measurement uncertainties associated with the pressure transducers, flow meter, wattmeter, and thermo-couples used in the experiment in Refs. [19] and [27] are 0.5%, 0.1%, 0.5%, and 0.3 K, respectively. The size of the geometric model of the experiment in the cited literature is close to that of the simulation model in our study. The characteristic lengths are both at the millimeter scale. The structures in Refs. [19] and [27] and this paper are both multi-hole jets with equal jet size, which is 0.42 mm for the diameter, 0.35 mm length and 0.2 mm width, respectively. Additionally, the dominant heat transfer mechanisms in both of the structures are the impinged convection in a confined space. And the experiment and simulation are both under single-phase flow and heat transfer regimes. Moreover, the effective heat flux of the experiment is 16.1–304.9 W/cm^2 and the heat flux of our study is 150 W/cm^2. Thus, the results in Refs. [19] and [27] can be used for the validation of the numerical model.

The working media is HFE7100 under single phase state and the thermophysical properties of HFE7100 used in our study is from Pan's work [28]. Considering that there is a small fluid temperature change, constant proporties was employed. Fig. 4 compares the simulation results with the experimental data according to pressure drop and thermal-couple temperature inside the copper heat sink. According to Fig. 4, the results show that the pressure drops from inlet to outlet have the same trend and very similar value between numerical results and experimental data under different inlet flow rate. Additionally, there are smaller variation slops of temperature from the center to outlet of channel than the experimental results, which may be caused by non-uniform flowrate over the jet slots along the channel. The inlet velocity boundary used in the numerical model results in the same flow rate of each jet. However, the flow rate is non-uniformly distributed over the jet slots in the experiment due to the different flow resistance of each jet stream. Therefore, the temperature increase from the center to the outlet of the channel is more obvious in the experiments. The standard k-ω model yields the good agreement with the experiments and considering the shear stress and mixed flow caused by the jet impingement, the standard k-ω model is selected.

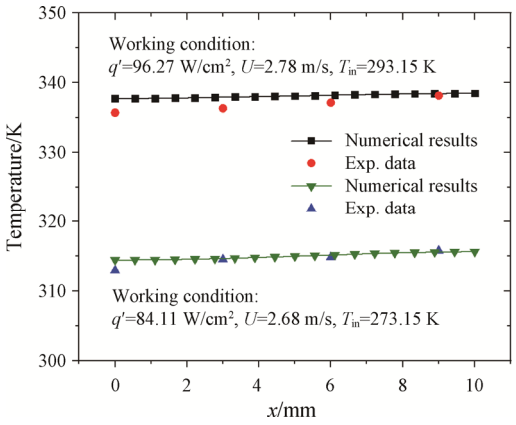

Fig. 4 Comparison of experimental data and simulation results of standard k-ω turbulence model

3. Results and Discussion

3.1 Effects of jet width

To study the jet width (W_{jet}) effect on the cooling performance, the heat flux and total flow rate are maintained at 1.5 MW/m^2 and 1 L/min, respectively, and L_{jet}, D_{imp}, L_{hpt} and W_s remain unchanged. When the jet width increases, the impinging velocity is reduced. As a result, the average temperature of the heating surface increases gradually from 309.1 K to 315.6 K as shown in Fig. 5(a). The results show that the variation of jet width has little influence on the uniformity of temperature

distribution (maximum temperature difference almost unchanged). Meanwhile, the thermal resistance increases from 6.05 K·m^2/MW to 10.38 K·m^2/MW. Due to the increased cross-section of impinging channel, pressure drop from inlet to outlet decreases as W_{jet} increases, especially from W_{jet}=0.1 to 0.2 mm. Although the lowest average heating surface temperature and thermal resistance can be obtained when W_{jet}=0.1 mm, the pressure drop is about one order of magnitude higher when W_{jet}=0.2 mm. Additionally, the pressure gradient between 0.1 mm and 0.2 mm is large (almost 169.3 Pa) while from 0.2 mm to 0.5 mm is smaller. The pumping power is 0.66 W when W_{jet}=0.2 mm and temperature of the cooling surface is in the acceptable range. Therefore, the optimal jet width of 0.2 mm is suggested.

To see Fig. 6(a), the heat is cooled through fluid-structure coupling surface which consists of impinged area and the micro-fin area. The base area of a fin is similar to the impinged area, while the total surface area of a fin is about 12 times of the impinged area. In order to elucidate the heat transfer pathways, it is necessary to compare the proportion of heat dissipation at the impingement area with that at the secondary heat transfer surface. Given the jet pitch, the increase of jet width leads to the decrease of the impinged velocity and the convective heat transfer rate at the impinged area. Although the increase of jet width increases the conduction area of the fin, the impinged velocity dominated, which lowers the fin efficiency. As a result, the proportion of micro-fin heat dissipation reaches the highest value of 37.5% when the jet width is 0.2 mm, and then it decreases as the jet width increases beyond 0.2 mm.

Fig. 7 shows the stagnation area and the variation of Nusselt number and Reynolds number under different jet width. Results show that the highest and lowest *Nu* are 112.4 and 62.1 when the jet widths are 0.1 mm and 0.5 mm, respectively. It can be concluded that W_{jet}=0.1 mm has the ability to dissipate the highest amount of heat because of the highest jet velocity among the cases and the Reynolds number also shows the highest value. It follows that reducing the jet width results in better heat transfer performance because as the Reynolds number increases, the degree of turbulence increases and the flow and heat transfer becomes more adequate. Fig. 8 shows the streamline of the fluid domain when the jet width is 0.3 mm. According to flow patterns, the fluid

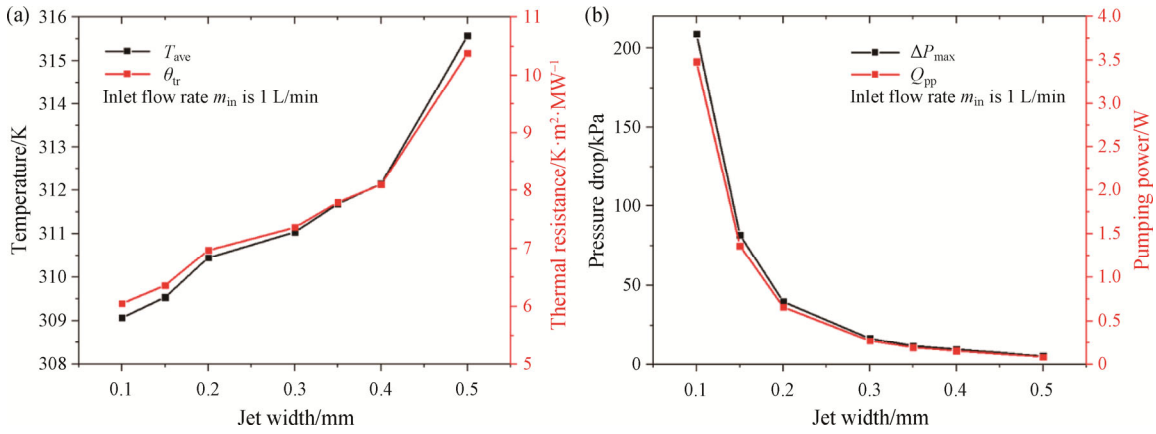

Fig. 5 Average heating surface temperature and thermal resistance (a); pressure drop and pumping power (b) under different jet width

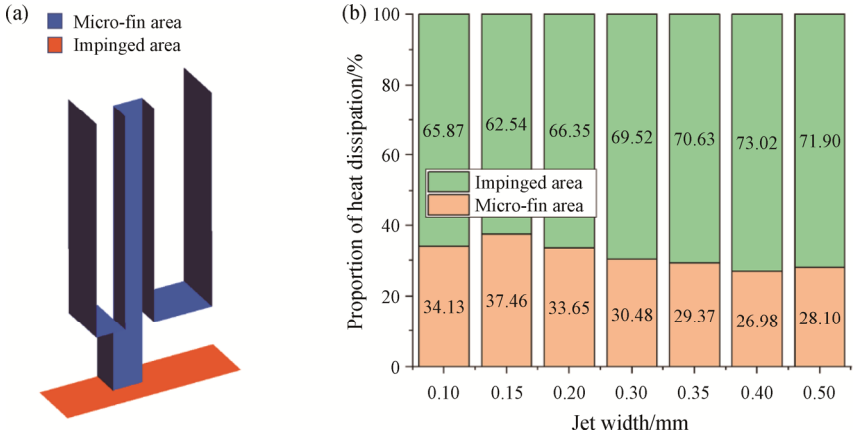

Fig. 6 Position (a) and the heat dissipation proportion (b) of micro-fin and impinged area under different jet width

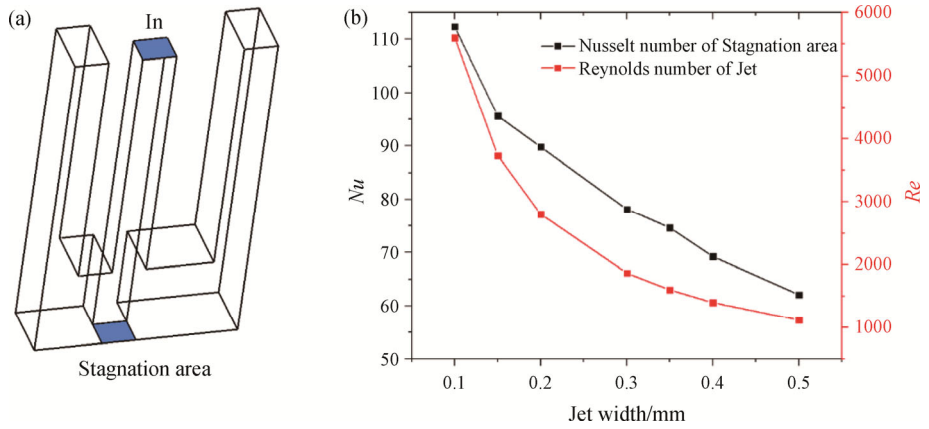

Fig. 7 Stagnation-area and Nusselt number of the stagnation area under different jet width

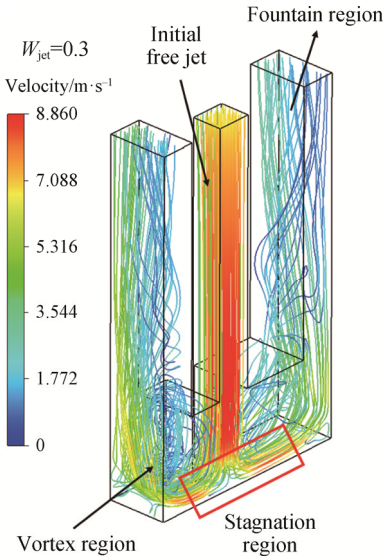

Fig. 8 Streamline of the fluid domain under different jet width

domain can be categorized into four regions: initial free jet region, stagnation region, vortex region and fountain region. As the cooling liquid flows into the jet inlet, the velocity increases along the jet channel until the flow is fully developed. And the liquid impinges onto the impined surface and then flows into the outlet channels separately. The jet velocity becomes zero when reaches the stagnation area, where the highest convective heat transfer coefficient and Nusselt number appear.

3.2 Effects of jet spacing

Given W_{js}=W_{jet}, the jet spacing determines the jet number per unit length and jet density. Simulations are performed with jet spacing from 0.1 mm to 0.5 mm when the heat flux and total flow rate remain at 1.5 MW/m^2 and 1 L/min, respectively. Fig. 9 shows the variations of thermal resistance, the average temperature, pumping power and the pressure drop under different the jet spacing. As the jet spacing increases, the average

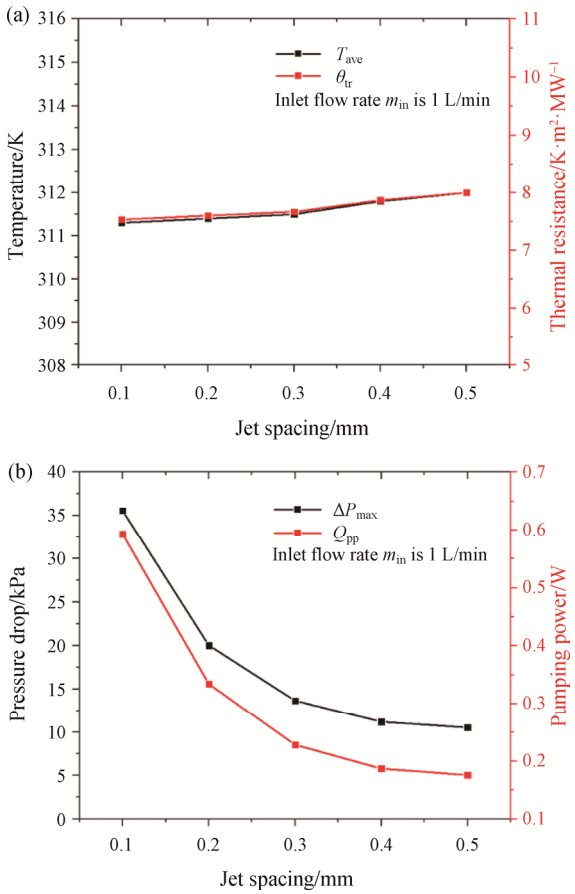

Fig. 9 Average heating surface temperature and thermal resistance (a); pressure drop and pumping power (b) under different jet spacing

temperature increases from 311.3 K to 312.0 K and the thermal resistance increases from 7.53 K·m^2/MW to 8.00 K·m^2/MW. As shown in Fig. 9(b), the effects of jet spacing on the pressure drop and pumping power are similar with that of the jet width. When W_{js} varies from 0.1 mm to 0.2 mm, the pressure drop decreases by 15.5 kPa; as W_{js} decreases to 0.5 mm, the pressure drop decreases by 9.5 kPa.

By reducing the jet spacing, the jet density is increased and the area of micro-fin heat cooling surface is increased, which can significantly enhance fin heat dissipation proportion. Fig. 10 shows the heat dissipation via fins accounts for 38.9% for W_{js}=0.1 mm. After the overall consideration, the best jet spacing for the jet impingement microchannel heat sink is 0.2 mm because the thermal resistance is small and the pressure drops significantly when W_{js} changes from 0.1 mm to 0.2 mm.

To see Fig. 11, Nusselt number of the stagnation area shows the downward trend as the jet spacing increases. The highest *Nu* is 98.9 for W_{js}=0.1 mm and the lowest *Nu* is 71.7 for W_{js}=0.5 mm indicating that the best cooling effect can be obtained when the jet spacing is 0.1 mm. When the whole heat sink width stays constant, the jet spcaing only determines the jet density of the heat sink. The inlet velocities are the same among all cases and changing the jet spacing has little effect on the influence of velocity on the heat cooling performance. As the above results show, when reducing the jet spacing, the jet density increases, and high ratio of micro-fin density can enlarge the heat transfer area; as a result, the thermal resistance of heat sink is small. Because the Reynolds number stays constant, the jet impact effect on cooling performance is the same, and the improvement of heat transfer ability depends on the micro-fin effect. Fig. 10 also illustrates that the micro-fin heat dissipation is the highest when jet spacing is 0.1 mm.

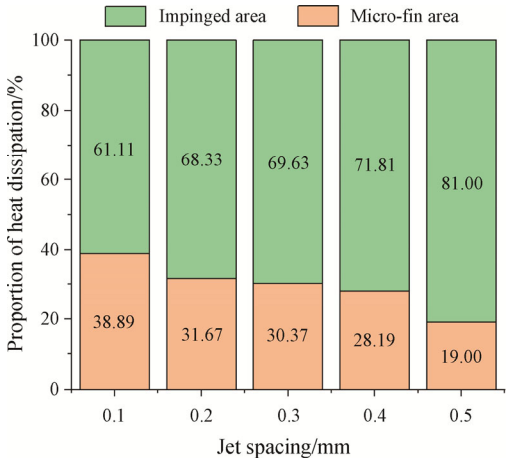

Fig. 10 The heat dissipation proportion of micro-fin and impinged area under different jet spacing

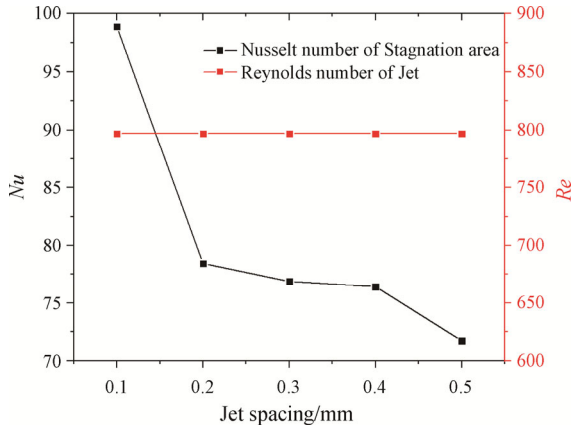

Fig. 11 Nusselt number of the stagnation area under different jet spacing

3.3 Effects of impingement distance

Jet impingement distance is also another crucial factor which has an influence on heat sink cooling ability. Fig. 12 shows the impingement distance (D_{imp}) effect on the heat dissipation ability of the proposed heat sink under the base working condition (1.5 MW/m^2 and 1 L/min). When the impingement distance increases from 0.1 mm to 0.9 mm, the average temperature of the heating surface increases by 1.5 K, and the thermal resistance increases from 7.33 to 8.33 K·m^2/MW. And when the jet distance increases from 1.0 mm to 3.0 mm, the average heating surface temperature increases by 3.7 K, and the thermal resistance increases from 13.8 to 20.6 K·m^2/MW. It can be seen that the pressure drop can be significantly reduced from 36.3 kPa to 12.5 kPa when the

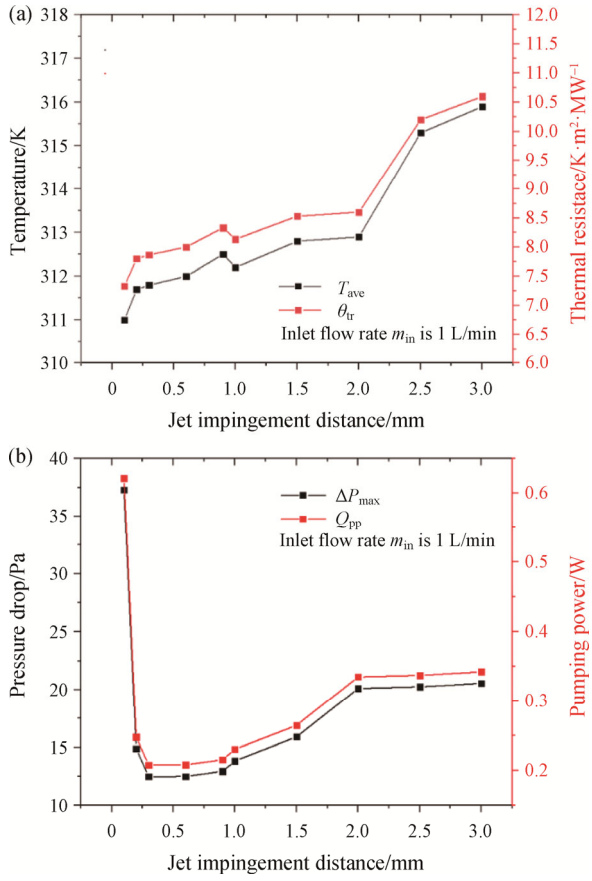

Fig. 12 Average heating surface temperature and thermal resistance (a); pressure drop and pumping power (b) under different impingement distance

impingement distance changes from 0.1 mm to 0.3 mm while it only increases by 8.1 kPa when the impingement distance increases from 0.5 mm to 3.0 mm. The pumping power line shows the similar trend. And in regard to the pressure drop and the heating surface temperature, the best jet impingement distance is 0.3 mm for the lowest pressure drop and pumping power.

Fig. 13 shows that the contribution of fins to the heat transfer becomes smaller at first (0.1 mm to 0.9 mm) and then becomes larger (1.0 mm to 3.0 mm) as the impingement distance increases. When the jet impingement distance increases from 0.1 mm to 0.9 mm, the jet impact effect on heat dissipation is obvious. Although the impact effect is the strongest when the jet impingement distance is 0.1 mm, the increased jet distance cannot significantly increase the fin heat dissipation surface (fin height increases due to the increase of D_{imp}), and most of the heat is still cooled by the impact surface. When D_{imp} varies from 1 mm to 3.0 mm, according to Fig. 15, the heat transfer proportion from the impact area becomes small because the inflow cannot directly impinge on the impact surface, and increasing the jet impingement distance can obviously enlarge the fin-dissipation area as the fin height increases.

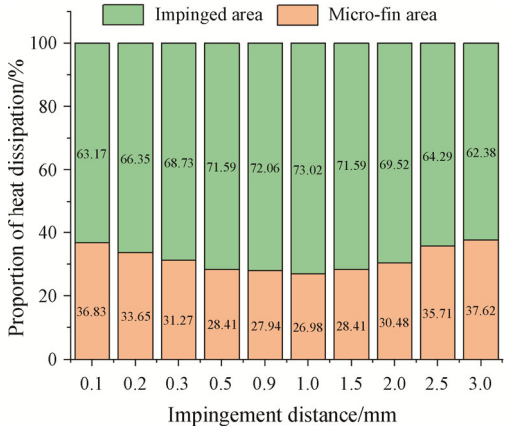

Fig. 13 The heat dissipation proportion of micro-fin and impinged area under different impingement distance

The average *Nu* number of the stagnation area on the impinged surface is shown in Fig. 14. The highest *Nu* number is 87.9 when D_{imp} is 0.1 mm while for D_{imp}=3.0 mm, the lowest value is 29.8. When D_{imp}<0.9 mm, *Nu* decreases as the impingement distance increases because the increase in jet impingement distance weakens the effect of jet impact effect. When D_{imp}>1.0 mm, *Nu* also decreases as the impingement distance increases but when D_{imp}=0.9 mm, *Nu*=76.6 and when D_{imp}=1.0 mm, *Nu*=76.7. The Reynolds number stays constant because changing the impingement distance has no effect on the Reynolds number of the inlet jet.

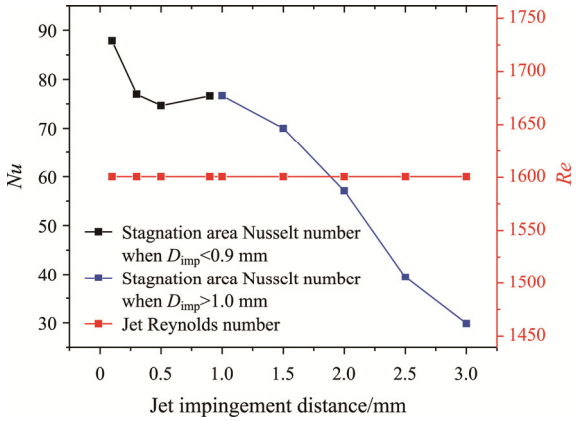

Fig. 14 Nusselt number of the Stagnation area under different impingement distance

Fig. 15 shows the velocity vector of flow field and it can be seen that the vortex area becomes bigger along with the increase of impingement distance, leading to the increase of thickness of the thermal fluid layer. A thicker layer of thermal fluid is not conducive to the full development of flow and heat transfer performance. When D_{imp}<0.9 mm, jet effect is weakened by the increase of jet impingement distance and the heat transfer performance becomes worse. According to Figs. 12 and 14, the Nusselt number decreases and the average temperature of the heating surface increases. When D_{imp}= 1.0 mm, the *Nu* number is 143.9% larger than when D_{imp}=0.9 mm. When D_{imp}<0.9 mm, the cooling performance mainly depends on the jet impact effect (it can also be explained by Fig. 14 that heat dissipation proportion of the impinged area decreases as D_{imp} increases), and when D_{imp}>1.0 mm, the cooling ability is mainly determined by the flow heat transfer. The fluid cannot directly impinge onto the impinged surface because the large vortex makes the jet flow direction offset and as a result, the heat cooling proportion by jet-impingement decreases as shown in Fig. 13. When D_{imp}=1.0 mm, the cooling effect depends on both the impingement heat dissipation and the flow and heat transfer by the thermal fluid vortex. The Nusselt number increases significantly compared with that when D_{imp}=0.9 mm which can be explained by the common heat transfer effect. The heat transfer characteristics in the heat sink will shift from impingement dominated heat transfer to the channel-convection dominated heat transfer as the jet impingement distance increases.

3.4 Effects of inlet flow rate

The inlet flow rate directly affects the jet Reynolds number, and the influence of flow rate on heat transfer characteristics is explored under conditions of a constant heating heat flux of 1.5 MW/m^2 and structure parameters of "0.35×1.5-0.5-1.0". In Fig. 16(a), both the heating surface average temperature and thermal resistace are

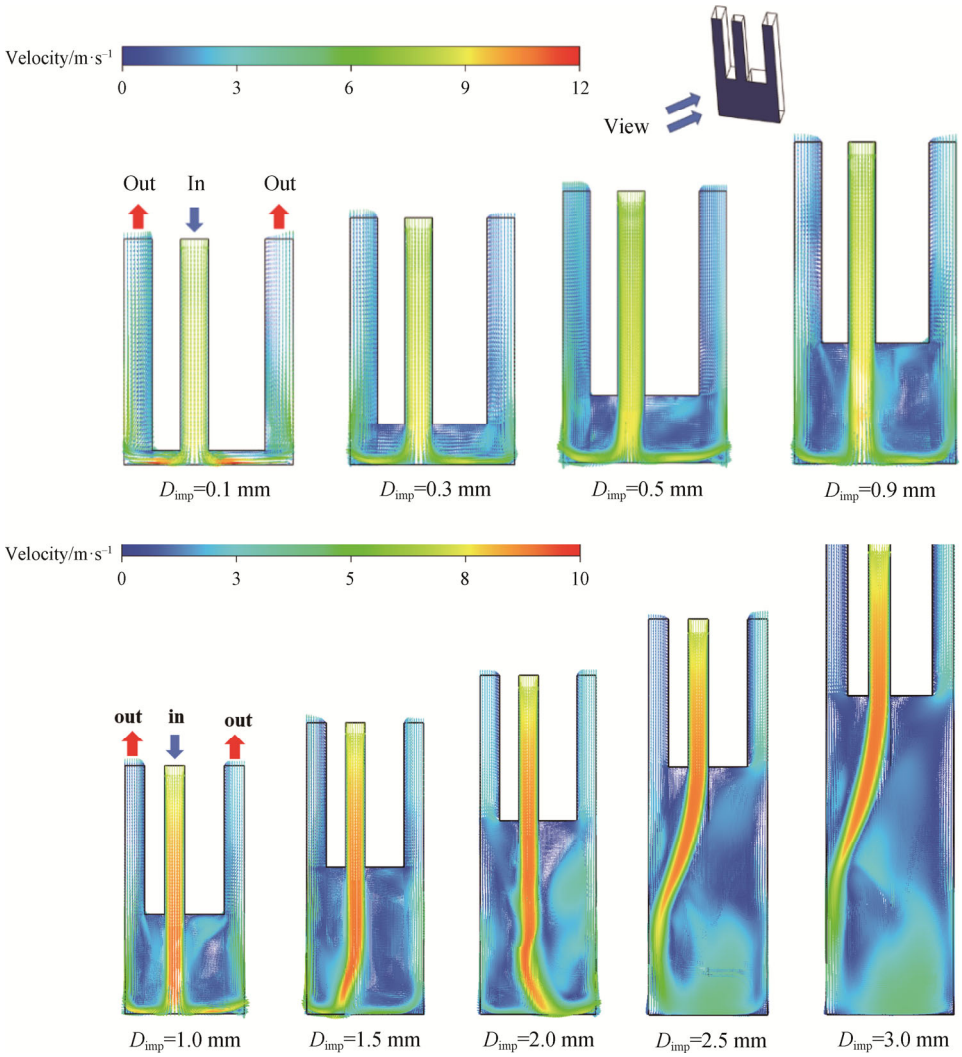

Fig. 15 Velocity vector diagram of the fluid domain under different impingement distance

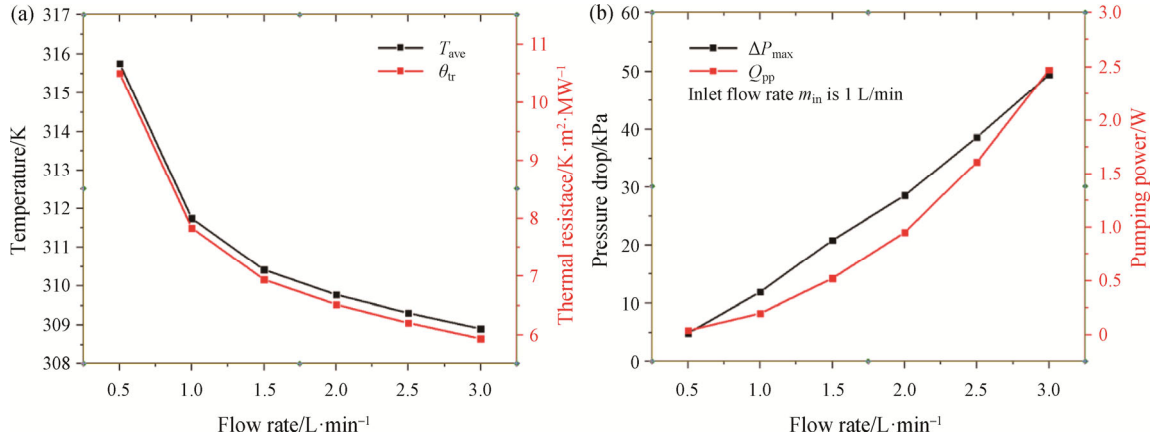

Fig. 16 Average heating surface temperature and thermal resistance (a), pressure drop and pumping power (b) under different flow rate

lowered by increasing the flow rate. From 0.5 L/min to 3.0 L/min, the average temperature is redeced from 315.8 K to 308.9 K and the thermal resistance is reduced from 10.5 K·m^2/MW to 5.9 K·m^2/MW. Fig. 16(b) shows that the pressure drop and the pumping power vary from 4.9 kPa to 49.4 kPa and 0.04 W to 2.47 W, respecticely.

Under the working condition of a flow rate of 3.0 L/min, the lowest thermal resistance is 5.9 K·m^2/MW.

Fig. 17 illustrates that the proportion of the heat dissipation rate of jet-impingement surface and micro-fin surface under different flow rate. The heat transfer proportion of micro-fin surfaces decreases from 38.1% to 23.3%. This is caused by the significant enhancement on the jet-impingement surface heat transfer as the impingement velocity increases. Fig. 18 shows the average *Nu* number of the stagnation-area and jet Reynolds number under different inlet flow rates. It is obvious that the Nusselt number and the Reynolds number can be increased from 55.9 to 85.5 and 800.3 to 4801.9 respectively, which indicates that the cooling effect can be enhanced by improving the inlet velocity.

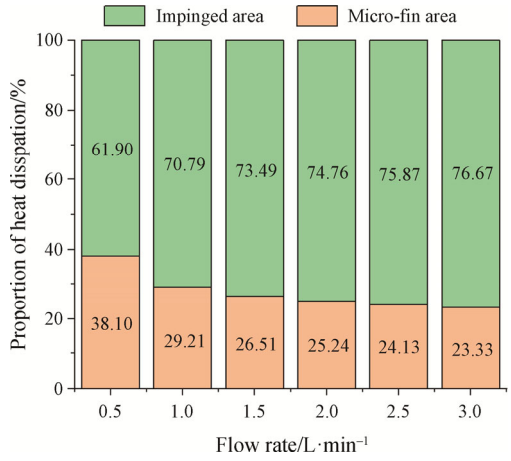

Fig. 17 The heat dissipation proportion of micro-fin and impinged area under different flow rate

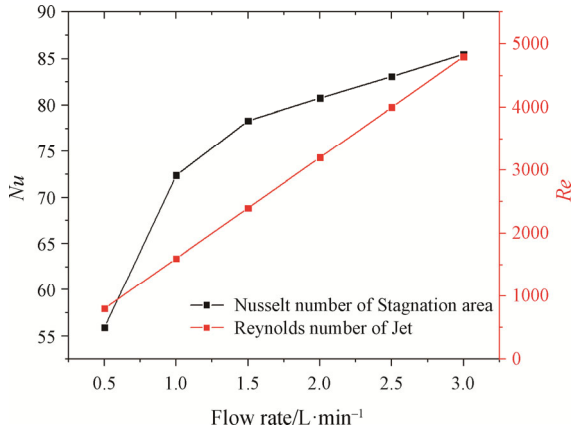

Fig. 18 Nusselt number of the stagnation area under different flow rate

3.5 Analysis of heat transfer characteristics of jet-impingement microchannel heat sink

Using the magnitude of thermal resistance as one critical criterion of flow and heat transfer performance, the present work further investigated the high heat flux (5 MW/m^2) dissipation ability of the proposed structure under different inlet flow rate. Fig. 19 compares the thermal resistace of the proposed structure in our work with that of the heat sinks from other works. It is obvoious that the proposed structure has thermal resistances significantly lower than most of the previous studies [19, 27, 29]. Our results are close to the optimical thermal resistances of heat sink with concave dimples proposed by Huang [30]. However, the pressure drop and surface temperatue variations in our study is much lower. The temperature homogeneity and low pressure drop of the proposed hybrid sink is owed to the dense arrangement of jet array which has a large total area of jet outlets (33.3% of the heating surface).

To study the flow and heat transfer mechanism of the jet impingement/microchannel heat sink with rectangular multi-array micro fins, Nusselt number of the axisymmetric jet flow at the stagnation area is an effective method for evaluating convective heat transfer intensity. According to the aforementioned numerical results of the parameter study, the single-phase data of the jet width, jet spacing, impingement distance and the flow rate were correlated as the following form:

$$\frac{Nu_0}{Pr^{0.4}} = aRe^b \cdot \left[c\left(\frac{H}{s}\right)^2 + d\left(\frac{H}{s}\right) + e \right] \cdot \left(\frac{W}{s}\right)^f \tag{9}$$

where, Nu_0 is the average Nusselt number of the stagnation area; the Prandtl number is constant in this study: 0.6; H is the impingement distance, which refers to D_{imp} in this article; W is the jet width, which refers to W_{jet} in this article; s is the copper plate thickness, which refers to D_p in this article (0.2 mm) as the characteristic length. The coefficients a, b, c, d and e are determined from a least-squares fitting to the numerical data, resulting in the following correlation. In this study, only

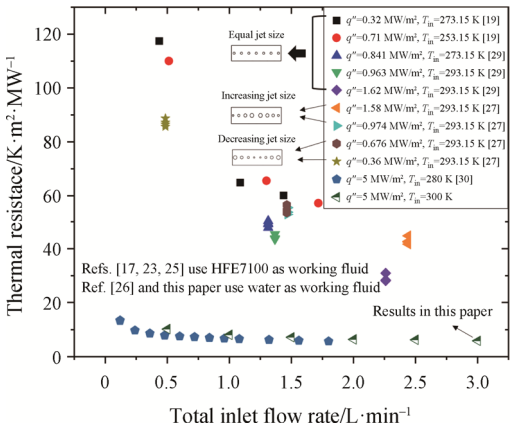

Fig. 19 Comparison of reseaches on the thermal resistance of different structure of hybrid jet-impingement/microchannel heat sink under different flow rate

water is considered as the working medium, and a constant Prandtl number is assumed as the fluid temperature variations are small.

When H/s belongs to the range of 0.5 to 4.5:

$$Nu_0 = 1.0553Re^{0.087\ 51} \cdot Pr^{0.4} \cdot \left[-2.7592\left(\frac{H}{s}\right)^2 + 4.5831\left(\frac{H}{s}\right) + 57.7371 \right] \cdot \left(\frac{W}{s}\right)^{-0.2369} \quad (10)$$

When H/s belongs to the range of 5.0–15.0:

$$Nu_0 = 0.6041Re^{0.0875} \cdot Pr^{0.4} \cdot \left[-0.3920\left(\frac{H}{s}\right)^2 + 2.1625\left(\frac{H}{s}\right) + 88.2325 \right] \cdot \left(\frac{W}{s}\right)^{-0.2369} \quad (11)$$

The R-square of this nonlinear regression model is 92.1% and 93.1% respectively, with almost all data points falling within a ±10% error range according to Fig. 20.

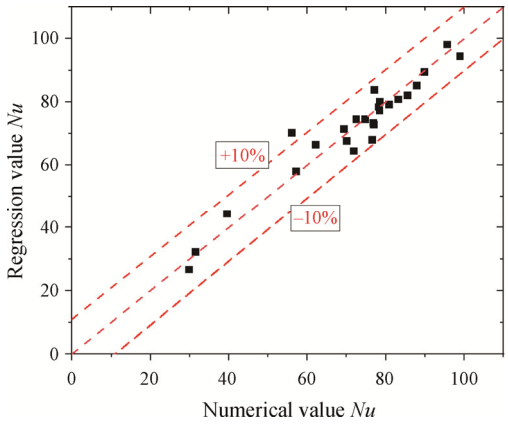

Fig. 20 Comparison of predictions on Nusselt number of stagnation area correlations and numerical data

4. Conclusions

A new type of jet-impingement microchannel heat sink with highly-dense jet array (~120 jets per cm^2) was proposed in this work, which can be applied to the cooling of high-power electronics. Parametric simulations are performed with single-phase water as coolant. The conclusions are summarized:

(1) The lowest thermal resistance of 5.9 K·m^2/MW among all cases is acheved at a 3.0 L/min flow rate with a pressure drop of 49.4 kPa under the heat flux of 1.5 MW/m^2.

(2) Owing to the design of a highly-dense jet array, heating surface temperature equilibrium can be obtained. The micro-fin structures in the hybrid heat sink can dissipate a large proportion of heat which accounts for 38.9% when the jet spacing is 0.1 mm.

(3) The parametric study on the structure optimization shows that the jet width, the jet spacing and the impingement distance have a remarkable influence on the cooling effect. Considering the trade-off between the pressure-drop and thermal resistance, the optimized jet width, jet spacing and impingement distance are 0.2 mm, 0.2 mm and 0.3 mm, respectively.

(4) A correlation of average Nusselt number of the stagnation-area is produced according to the numerical results of the parameter study of the flow and heat transfer performance of jet impingement microchannel heat sink.

Acknowledgements

This research was funded by the National Natural Science Foundation of China (52176020), and the Youth Innovation Team of Shaanxi Universities.

Conflict of Interest

On behalf of all authors, the corresponding author states that there is no conflict of interest.

References

[1] Pasupuleti T., Kandlikar S.G., Cooling of microelec-tronic devices packaged in a single chip module using single phase refrigerant R-123. ASME 2009 7th International Conference on Nanochannels, Microchannels, and Minichannels, 2009, Paper No: ICNMM2009-82262.

[2] Tuckerman D.B., Pease R.F.W., High-performance heat sinking for VLSI. IEEE Electron Device Letters, 1981, 2(5): 126–129.

[3] Zhang Y., Wang S., Ding P., Effects of channel shape on the cooling performance of hybrid micro-channel and slot-jet module. International Journal of Heat & Mass Transfer, 2017, 113: 295–309.

[4] Pandey J., Ansari M.Z., Husain A., Performance analysis of hybrid microchannel heat sink for varying nozzle geometry and layout on the basis of first- and second-law of thermodynamics. Journal of Mechanical Science and Technology, 2021, 35(12): 5753–5764.

[5] Zunaid M., Husain A., Chauhan B.S., et al., Numerical analysis of inclined jet impingement heat transfer in microchannel. Materials Today: Proceedings, 2021, 43: 557–563.

[6] Shen S., Xu J.L., Zhou J.J., et al., Flow and heat transfer in microchannels with rough wall surface. Energy Conversion & Management, 2006, 47(11–12): 1311–1325.

[7] Gan T., Ming T., Fang W., et al., Heat transfer enhancement of a microchannel heat sink with the

combination of impinging jets, dimples, and side outlets. Journal of Thermal Analysis and Calorimetry, 2019, 141(1): 45–56.

[8] Shokouhmand H., Aghvami M., Afshin M.J., Pressure drop and heat transfer of fully developed, laminar flow in rough, rectangular microchannels. ASME 2008 6th International Conference on Nanochannels, Microchannels, and Minichannels, 2008, Paper No: ICNMM2008-62042.

[9] Lee P.S., Teo C.J., Heat transfer enhancement in microchannels incorporating slanted grooves. ASME 2008 First International Conference on Micro/Nanoscale Heat Transfer, 2008, Paper No: MNHT2008-52374.

[10] Baghernezhad N., Abouali O., Numerical investigation of single phase heat transfer enhancement in a microchannel with grooved surfaces. ASME 2008 6th International Conference on Nanochannels, Microchannels, and Minichannels, 2008, Paper No: ICNMM2008-62262.

[11] Solovitz S.A., Computational study of grooved microchannel enhancements. ASME 2008 6th International Conference on Nanochannels, Microchannels, and Minichannels, 2008, Paper No: ICNMM2008-62128.

[12] Vanapalli S., Brake H.J.M.T., Jansen H.V., et al., Pressure drop of laminar gas flows in a microchannel containing various pillar matrices. Journal of Micromechanics & Microengineering, 2007, 17(7): 1381.

[13] Kuppusamy N.R., Saidur R., Ghazali N.N.N., et al., Numerical study of thermal enhancement in micro channel heat sink with secondary flow. International Journal of Heat and Mass Transfer, 2014, 78(3): 216–223.

[14] Wu Z., Zhu H., Gao Q., et al., Experimental and numerical investigation of impingement heat transfer on target plate with streamlined roughness element at maximum crossflow condition. Journal of thermal science, 2022, 31: 751–764.

[15] Kandlikar S.G., Review and projections of integrated cooling systems for three-dimensional integrated circuits. Journal of Electronic Packaging, 2014, 136(2): 024001.

[16] Zhang Y.J., Wang S.F., Liu Z.M., Effect of fluid distribution on the cooling performance of hybrid microchannel and slot-jet impingement system. Applied Thermal Engineering, 2023, 222: 119913.

[17] Deshpande M.D., Vaishnav R.N., Submerged laminar jet impingement on a plane. Journal of Fluid Mechanics, 2006, 114: 213–236.

[18] Smakulski P., Pietrowicz S., A review of the capabilities of high heat flux removal by porous materials, microchannels and spray cooling techniques. Applied Thermal Engineering, 2016, 104: 636–646.

[19] Sung M.K., Mudawar I., Single-phase and two-phase hybrid cooling schemes for high-heat-flux thermal management of defense electronics. 2008 11th Intersociety Conference on Thermal and Thermomechanical Phenomena in Electronic Systems, IEEE, 2008. DOI: 10.1109/ITHERM.2008.4544262

[20] Sung M.K., Mudawar I., Experimental and numerical investigation of single-phase heat transfer using a hybrid jet-impingement/micro-channel cooling scheme. International Journal of Heat and Mass Transfer, 2006, 49(3–4): 682–694.

[21] Chen W.J., Wong K.C., Ng K.C., Effect of adding fillet to protruded rectangular rib in a microchannel heat sink subject to jet impingement cooling. Enabling Industry 4.0 through Advances in Manufacturing and Materials, Lecture Notes in Mechanical Engineering, Springer, Singapore, 2022, pp: 227–236.

[22] Cui H.C., Lai X.T., Wu J.F., et al., Overall numerical simulation and experimental study of a hybrid oblique-rib and submerged jet impingement/microchannel heat sink. International Journal of Heat and Mass Transfer, 2021, 167(4): 120839.

[23] Jang S.P., Kim S.J., Paik K.W., Experimental investigation of thermal characteristics for a microchannel heat sink subject to an impinging jet, using a micro-thermal sensor array. Sensors & Actuators A: Physical, 2003, 105(2): 211–224.

[24] Lelea D., The microtube heat sink with tangential impingement jet and variable fluid properties. Heat and Mass Transfer, 2009, 45(9): 1215–1222.

[25] Loganathan R., Gedupudi S., Numerical studies on single-phase micro-channel heat sink with multiple inlets along the channel. ICHMT Digital Library Online, 2017. DOI: 10.1615/ICHMT.2017.CHT-7.1770.

[26] Revill B.K., Mixing in the process industries, Chapter 9—Jet mixing. Edited by: Harnby N., Edwards M.F., Nienow A.W., Butterworth-Heinemann, 1992, pp: 159–183.

[27] Sung M.K., Mudawar I., Effects of jet pattern on single-phase cooling performance of hybrid micro-channel/micro-circular-jet-impingement thermal management scheme. International Journal of Heat and Mass Transfer, 2008, 51(19–20): 4614–4627.

[28] Pan Y., Zhao R., Nian Y., et al., Study on the flow and heat transfer characteristics of pin-fin manifold microchannel heat sink. International Journal of Heat and Mass Transfer, 2022, 183: 122052.

[29] Sung M.K., Mudawar I., Single-phase and two-phase heat transfer characteristics of low temperature hybrid micro-channel/micro-jet impingement cooling module. International Journal of Heat and Mass Transfer, 2008, 51(15–16): 3882–3895.

[30] Huang X., Wei Y., Ming T., et al., Heat transfer enhancement on a microchannel heat sink with impinging jets and dimples. International Journal of Heat and Mass Transfer, 2017, 112: 113–124.